

Spreading of a thin wetting film: Microscopic approach

S. F. Burlatsky,^{1,*} G. Oshanin,² A. M. Cazabat,³ M. Moreau,² and W. P. Reinhardt¹

¹*Department of Chemistry BG-10, University of Washington, Seattle, Washington 98195*

²*Laboratoire de Physique Théorique des Liquides,[†] Université Paris VI, 4 Place Jussieu, 75252 Paris Cedex 05, France*

³*Laboratoire de Physique de la Matière Condensée,[‡] Collège de France, 11 Place Marcelin Berthelot, 75231 Paris Cedex 05, France*

(Received 5 October 1995; revised manuscript received 14 February 1996)

In this paper we present a microscopic model description of spreading kinetics of a monomolecularly thin wetting film climbing from a bath of liquid along a vertical solid wall. We find analytically that both the linear extension and the mass (number of particles) of the film grow in proportion to \sqrt{t} , in accord with experimental observations. We also analyze the details of the fine structure of the wetting film and determine explicitly the concentration profile along the film and concentration gradients at the tip of the film and in the vicinity of the liquid bath. We show that the essential physical mechanism responsible for film's growth is associated with the diffusive transport of vacancies from the tip of the film to the liquid bath, where they are filled with fluid particles. [S1063-651X(96)04309-7]

PACS number(s): 68.15.+e, 05.40.+j, 68.45.Gd

I. INTRODUCTION

Spreading of liquid droplets on surfaces and fibers plays a crucial role in numerous technologies including lubrication, painting, coating, emulsion, dyeing, gluing, and oil recovery from porous rocks [1–5]. In all cases, efficient practical applications require precise knowledge of the conditions and laws of spreading. For macroscopically large drops the spreading kinetics are well described by continuum hydrodynamic theories that ignore the molecular structure of liquids. The evolution of such properties of macroscopic drops as the size of the macroscopic liquid edge, the height, the profile, and the contact angle is presently well understood and is described by the universal Tanner law and its extensions [1–12]. In contrast, the origin of universal laws that seemingly govern spreading dynamics at the microscopic scale, as evidenced by recent experimental works [13–15], still remains unclear [16].

The salient features at the microscopic, molecular scale is the appearance of a liquid film, the precursor [17], which is pulled out of the drop by unbalanced capillary forces. This precursor, whose thickness may vary from several (molecular size) to a few hundreds of angstroms, precedes the macroscopically observable liquid edge and the drop then actually spreads on top of this film. The linear extension h_t of the film at sufficiently large times may be macroscopically large.

Refined ellipsometric measurements [13–15, 18–20] have scrutinized the growth of the precursor film and reached a rather surprising conclusion: h_t obeys a universal law $h_t \propto \sqrt{t}$, regardless of the nature of the species involved. This growth law has been observed for various substrates and also for various kinds of liquids: simple, polymeric, and surfactant melts. For some substrates a remarkable effect of “terrace spreading” takes place—several monolayers advance

together stacked on top of one another and each growing as \sqrt{t} [13–15]. For capillary rise geometries, in which a vertical wall is put into a contact with a bath of liquid, a film of microscopic thickness (or sometimes several monolayers [21]) rises from the macroscopic meniscus and creeps upwards along the wall. In this case the length of the film increases in proportion to \sqrt{t} within an extended time domain [22,23], until the film's growth is truncated at very high altitudes due to gravity [8,9]. Finally, recent experimental studies (see also Sec. V for more detailed description) of spreading of metallic beads on a horizontal vibrating racklike surface [24] found a \sqrt{t} law for growth of the area covered by the beads, thus showing that such a behavior is not a specific feature of spreading liquids, but is relevant to a wider range of systems. Therefore, the \sqrt{t} law is independent of the nature of the substrate and of the liquid, as well as of the geometry, intermolecular interactions and also of the size of molecules, which can be even macroscopically large as in the case with beads. The prefactors in this law depend, of course, on the particular situation under study.

Theoretical studies of this phenomenon have been largely numerical. In particular, in [25] the $h_t \propto \sqrt{t}$ law for the growth of the precursor was reproduced in the molecular dynamics (MD) simulations involving Lennard-Jones molecules. The MD simulations in [26,27], which differ from [25] in the model of the substrate, displayed the spreading in the form of different monolayers stacked on top of one another, but showed, however, the $h_t \propto \sqrt{\log(t)}$ growth of monolayers [28]. In [29,30], which was concerned with MD simulations of systems with Lennard-Jones chainlike molecules, “terrace spreading” in the form of distinct layers with their radii growing as \sqrt{t} was found. Finally, in [31] an Ising-type lattice-gas model was employed instead of the molecular dynamics, which has also demonstrated the \sqrt{t} law for growth of the precursor length. Following the trajectories of tracer particles, it was deduced [31] that this behavior occurs due to migration of second layer particles to the holes in the perimeter of the precursor. Details of this and earlier numerical works were recently summarized in [16].

*Present address: LPTL, Université Pierre et Marie Curie, 4 Place Jussieu, 75252 Paris Cedex 05, France.

[†]Unité de Recherche Associée au CNRS (URA 765).

[‡]Unité de Recherche Associée au CNRS (URA 792).

Meanwhile, several theoretical developments aimed at the explanation of the origin of the \sqrt{t} law have occurred. In [8] a continuum hydrodynamic theory was developed, which derived the \sqrt{t} law from the diffusive motion with inhomogeneous diffusion coefficient dependent on the local disjoining pressure [1]. This theory presumes, however, that the film thickness remains at least in the mesoscopic range, where the continuum hydrodynamics description is still appropriate [8]. Thus this approach does not explain the growth of monolayers; thin films cannot be viewed as a true liquid phase and actually they often show solidlike or glassy behaviors [32–36]. In [6,22,23] the hydrodynamic description in [8] was extended down to the microscopic scale, adopting basic equations of [8], but assuming a different origin of frictional forces.

A qualitatively different approach has been proposed in [37], which viewed the liquid drop as a completely layered structure, each layer being a thin incompressible two-dimensional fluid of small molecules. Permeation of the molecules perpendicular to the layers is allowed and takes place only in a “permeation ribbon” near the edges of successive layers. (Recent numerical simulations [38] show that this is actually so for strongly corrugated substrates.) Consequently, the layers may grow by the accretion of molecules at their edges from the layers above and below. The fluid particles do interact with the substrate in a manner that makes the lowest layers energetically more favorable and causes their growth. This picture yields the correct growth law of the advancing monolayers at long times, when one expects the difference between the radii of neighboring layers to be large. However, an assumption of incompressibility leads to serious problems in the analysis of the short time regimes. Additionally, the macroscopic hydrodynamic description of dissipative forces employed in [37] requires more detailed microscopic justification [1].

Lastly, in [39–41] an interesting nonequilibrium statistical physics approach has been devised, which made use of the solid-on-solid-model (SOSM) approximation [42]. In [39,40] the analysis focused on the Langevin dynamics of the drop’s interface (which is spatially coarse grained in the spirit of the SOSM) due to the surface tension and to the driving (capillary) force in the vicinity of the substrate. In this approach an extraction of precursor film has been established and also the dynamical profiles have been determined explicitly. This approximation, however, gives a precursor advancing at a constant speed, i.e., $h_t \propto t$, which contradicts the experimentally observed behavior. To avoid this inconsistency a different, “columnar” version of the SOSM has been employed [41], which takes into account entropic repulsion effects, but, nonetheless, a film extending linearly in time was found.

In this paper we present a microscopic model description of spreading and of the fine structure of monomolecularly thin films. We focus here on systems with the so-called planar geometry [6,22,23], i.e., on systems in which the film’s thickness (or concentration of particles in the film in case of monolayers) varies effectively only along one spatial coordinate. This typical experimental situation occurs when a solid, which may be a plane (Fig. 1) or a cylindrical fiber (Fig. 2), is immersed in a liquid bath. Here the particle concentration in the liquid film, which extracts from the macroscopic me-

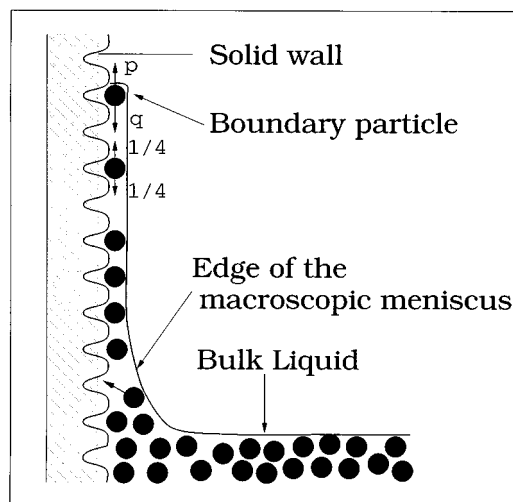


FIG. 1. A schematic picture of the standard capillary rise geometry. A vertical solid plane is immersed into the bath of liquid.

niscus and climbs along the solid, varies only with the altitude above the edge of the macroscopic meniscus and is independent of the perpendicular, horizontal coordinate.

Our model consists of three basic points: We suppose that the concentration of fluid particles at the edge of the static macroscopic meniscus is constant. Second, we view the motion of particles in the film on the solid surface as an activated random hopping, constrained by hard-core interactions, in spatially modulated potential. Third, here we ignore effects of gravity and also assume that all particles, except the ones at the tip of the film (Figs. 1 and 2)—the boundary particles (BP)—have symmetric transition rates. The hopping rates of the BP are asymmetric with the preferential direction towards the edge of the macroscopic meniscus. The origin of such asymmetry will be made clear below. Similar microscopic approaches were succinctly presented in [43,44], which concerned the dynamics of creep motion of an ultrathin film and lattice gas spreading, respectively. Mathematical aspects of the model presented here are akin to

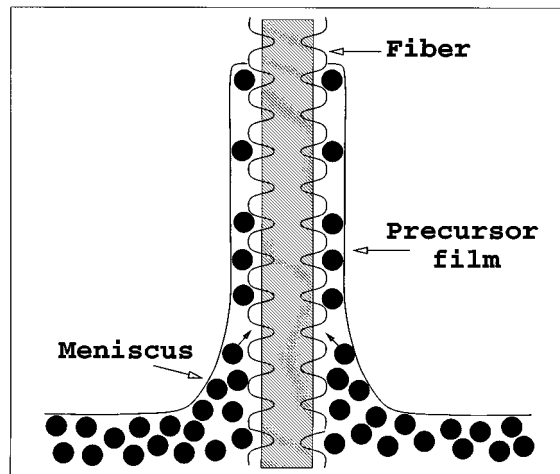


FIG. 2. Thin wetting film climbing on a cylindrical fiber from the bath of liquid.

the description of charged particle motion in a one-dimensional hard-core lattice gas in the presence of an external electric field [45,46]. Here the mean displacement of the charged particle grows in proportion to \sqrt{t} in the case of both infinitely large [45] and finite fields, and also for different types of boundary conditions [46].

In our microscopic approach we establish analytically the \sqrt{t} law for the growth of the film length and the mass (number of particles in the film) and determine explicitly the prefactors in this law. We also calculate the behavior of several characteristic properties, including the concentration profile along the film, the particle concentration and concentration gradient at the tip of the film. Additionally, we analyze the spreading kinetics in the case of strongly volatile liquids, when the surface tension of the liquid-vapor interface is negligibly small. In this case, which is also appropriate to experiments with spreading of metallic beads on a vibrating corrugated plane [24] we find that the length of the film (or the area covered by the beads) grows in time as $\sqrt{t \log(t)}$. The mass of the film (or the total number of particles) is found to obey, however, the \sqrt{t} law without logarithmic corrections.

The paper is structured as follows: In Sec. II we describe the microscopic model of spreading kinetics. In Sec. III we formulate the corresponding one-dimensional stochastic process and derive basic equations. In Sec. IV we analyze solutions of these equations in situations appropriate to spreading of liquids with well-developed liquid-vapor interface and compare our analytical results against the results of numerical simulations. In Sec. V we analyze the growth of a monolayer in the case of strongly volatile liquids. Finally, in Sec. VI we conclude with a summary and discussion.

II. THE MODEL

Our model, which will be presented in the Secs. II A–II C, is relevant to the following experimental situation. Suppose that a vertical solid wall is immersed in a bath of liquid. The liquid interface, which is initially horizontal, changes its shape in the vicinity of the solid wall and a macroscopic meniscus builds up (see Figs. 1 and 2). The size of the macroscopic meniscus (both horizontally and vertically) is comparable to the capillary length. After a suitable transient period a thin liquid film exudes from the static macroscopic meniscus and climbs up the solid wall. The growth of films whose thickness is in the mesoscopic range has been described in terms of a continuum hydrodynamic theory in [8]. In the present paper we are concerned with the properties of molecularly thin films.

A. Concentration at the edge of the macroscopic meniscus

We consider the liquid bath as a reservoir of particles (of an infinite capacity), which maintains a constant concentration C_0 of fluid particles at the edge of the macroscopic meniscus (EMM). We estimate C_0 as follows: Suppose that one has a vacancy directly at the EMM (see Figs. 1 and 2) and a fluid particle (particle with an arrow in Figs. 1 and 2) in the volume of the macroscopic meniscus, which can jump onto this vacancy within one step. Let us denote now as E_{\downarrow} the energy gained by moving this particle onto the vacancy.

Then, employing essentially the same reasonings as those used in the derivation of Langmuir adsorption isotherm [47], we calculate C_0 , which in the limit $\beta E_{\downarrow} \gg 1$, $\beta = 1/kT$, takes the simple form

$$C_0 \approx 1 - \exp(-\beta E_{\downarrow}). \quad (1)$$

The value of E_{\downarrow} is dominated by two factors. The positive contribution to E_{\downarrow} comes from the presence of attractive interactions between the fluid particles and the solid wall and can be readily defined through the parameters of these interactions. The second, negative factor is a loss of energy due to the breaking of bonds with several fluid molecules, since for the particles in the volume of the meniscus the number of neighbors is greater than that for particles directly on the solid. We note, however, that this factor is not independent of particle-substrate interactions; the concentration profile and thus the number of neighboring molecules depend significantly on the strength of interactions with the substrate.

We also stress that when C_0 is not too small (of order of unity), equilibration of the concentration at the EMM is a very rapid process; the approach of concentration to its equilibrium value, Eq. (1), is exponentially fast. As we set out to show, relaxation processes in the film proceed on an essentially slower time scale and are described by power laws. We thus neglect the variation of C_0 in time and assume in what follows that the concentration at the EMM is constant and given by Eq. (1).

B. Dynamics of particles on the solid wall

Consider next particle dynamics on the solid surface. We make use of the conventional picture of such dynamics and view the motion of particles as an activated random hopping transport, constrained by hard-core interactions, between the local minima of a waferlike array of potential wells. Such wells occur because of the mutual interactions of particles in the film (as for the motion in bulk liquids) and also because the film's particles experience short-range forces exerted by the atoms of the solid. Consequently, the interwell distance a may be related either to the radius of the repulsive part of the particle-particle interactions or to the spacing between the atoms of the substrate. Without going into details of particle-particle and particle-substrate interactions, we suppose that for the transition to one of the neighboring potential wells a particle has to overcome a potential barrier. This barrier does not create a preferential hopping direction, but results in a finite time interval τ between the consecutive hops, defined through the Arrhenius formula. We note also that such a picture of particle motion presumes a certain assumption about the nature of the dissipative forces [1]; the stick-and-slip motion model adopted here means that a particle loses velocity completely after one jump.

To specify the positions of the wells, we introduce a pair of perpendicular coordinate axes (X, Y) , where X is a vertical coordinate, which measures the altitude of a given well above the EMM (Fig. 1), while Y defines the horizontal position of this well.

We assume that all particles (except the boundary particles, which among all the particles at a given moment of time and fixed Y have the maximal altitude $X = h_t$) have symmetric transition rates: for these a probability of hop in

any of four directions is $1/4$. Then, the diffusion coefficient of particles on the solid is defined through the parameters a and τ as $D = a^2/4\tau$. In physical terms we may rewrite this as $D = kT/\gamma$, where k and T are the Boltzmann constant and the temperature, respectively, while γ is the effective friction coefficient for motion in a liquid monolayer on the solid wall. Hard-core interactions constrain the particle hopping motion; no two particles can simultaneously occupy the same well. Thus a hop into an occupied well is forbidden.

C. Dynamics of the boundary particles

Now we define dynamics of the BP, which will be different from that of particles in the film. First, for the BP the hops down to the EMM and hops along the horizontal axis are constrained by hard-core interactions, while upward hops are unconstrained since wells above $X = h_t$ are always vacant. Second, motion of the BP along the X axis is asymmetric—we stipulate that upward hops occur with smaller probability (p) than downward hops (q), $p < q$.

Such an asymmetry may be roughly illustrated in terms of the SOSM approximation [39–41]. In this model the cost of interfacial energy F for having a film of length h_t (Figs. 1 and 2) is $F = Jh_t$, where the prefactor J is related to the surface tension of the liquid-vapor interface. This means that the interface exerts a *constant*, independent of the film's length, pressure on the film directed towards the EMM, or in other words, the BP experience an action of a constant force f , $f = -\partial F/\partial h_t = -J$, which favors its hops downwards to the EMM. Let us stress that in this picture only the boundary particle is subject to a surface-induced force; all other particles in the film do not “feel” the presence of the interface and thus have symmetric transition rates.

The microscopic origin of the asymmetric hopping rates stems from the mutual interactions between the particles in the film. Typical interactions in real systems are characterized by a harsh repulsion of a hard-core type at short scales and attraction at longer distances. Now, upward and downward hops of the BP do not change the number of particles at a given Y but result in stretching or shrinking of the film. Thus the change in the length of the film comprising a fixed number of particles results in the change of energy. Stretching of the film (an upward hop of the BP) will lead to an increase of energy. Conversely, shrinking of the film decreases the interparticle distances and thus results in a decrease of energy. In other words, the presence of particle-particle attraction results in correlations between the local transition rates and spatial distribution of particles—these tend to move towards the spatial regions in which the particle concentration is high. Since the concentration is maximal at the EMM and decreases with an increase of altitude the particles in the film experience, on average, an action of a force that is directed to the EMM. In our model this circumstance will be taken into account by introducing an integral (over all particles of the film) force that acts on the BP only and that is equivalent to the presence of a SOSM-type interface with some effective surface energy W_- . In view of previous discussion we will define W_- , which is the difference of the energies lost and gained due to the upward and downward hops of the BP, as the work required to transport a vacancy from the tip of the film to the EMM. Using de-

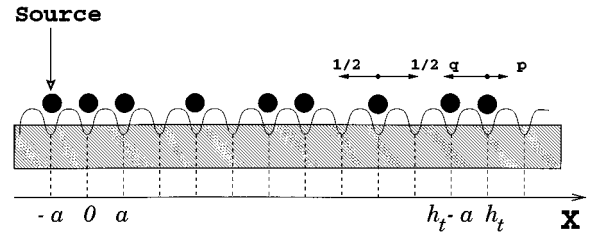


FIG. 3. Illustration of a stochastic process describing motion of particles on the solid wall.

tailed balance arguments we get the following relation between p , q , and W_- :

$$\frac{p}{q} = \exp(-\beta W_-). \quad (2)$$

We note, finally, that by definition W_- equals the difference of the potential energy of vacancy placed at the EMM and the potential energy of vacancy at the tip of the film, and hence is independent of the length and the mass of the film, provided that $h_t \gg a$.

III. BASIC EQUATIONS

Now we turn to the mathematical description of the film growth defined by Secs. II A–II C. We introduce the variable $\eta(X, Y, t)$, the time-dependent occupation variable of the well with coordinates X and Y , which equals 1 if the well is occupied and 0 if the well is empty. We note next that the dependences of $\eta(X, Y, t)$ on the X and the Y coordinates have quite different origins. There is a reservoir of particles, which maintains fixed occupation of all wells at $X = -a$, and a well-defined constant force acting on the BP's along the X axis. Consequently, we may expect a regular X dependence of $\eta(X, Y, t)$. In contrast, the Y dependence may be only noise; the uniform boundary at the EMM ensures that there is no regular dependence on the Y coordinate and only the particle dynamics may cause fluctuations in $\eta(X, Y, t)$ along the Y axis. In the present paper we will disregard these fluctuations and suppose that the occupation variable varies along the X axis only, i.e., $\eta(X, Y, t) = \eta(X, t)$. Consequently, we will have an effectively one-dimensional problem in which the presence of the Y direction will be accounted for only through the particles' dynamics. We note finally that the assumption of such a type is, in fact, quite consistent with experimental observations [13–15], which show that in the case of sufficiently smooth substrates and liquids with low volatility the width of the film's front is very narrow.

Then, in neglect of the fluctuations along the Y axis the variable $\eta(X, t)$ can be viewed as a local time-dependent variable describing occupation of the site X in a *stochastic process* in which hard-core particles perform hopping motion (with the time interval τ between the consecutive hops) on a one-dimensional lattice of spacing a (see Fig. 3). All particles, except the BP, have probabilities $1/4$ for hops from X to $X \pm a$, and probability $1/2$ to stay at X (arising from the motion along the Y axis). The BP, being at X , may jump to $X + a$ with probability p and to $X - a$ with probability q ,

provided that this site is vacant, and may remain at X with probability $1/2$. Further on, a source at $X = -a$ maintains a fixed occupation of this site. This process is a generalization of a “directed walk in a lattice gas” model, studied analytically and numerically in [45,46], and here we will extend the previously elaborated continuous-space and time mean-field-type description to the more complicated process under study. In this description we will focus on the evolution of the BP mean displacement, which we denote as h_t , and mean occupation (or concentration) of the site X at time t , $C(X,t) = \langle \eta(X,t) \rangle$, where brackets denote averages with respect to different realizations of the stochastic process. The analytical results will be afterwards (in Sec. IV C) compared to the results of Monte Carlo simulation of the discrete space and time stochastic process.

We start with the dynamics of the BP. Its mean displacement obeys the following exact equation:

$$\tau \frac{dh_t}{dt} = ap - aq(1 - C_1), \quad (3)$$

where $C_1 = C(X = h_t - a, t)$, i.e., the mean occupation of the site adjacent to the position of the BP. Equation (3) shows that hops away from the EMM occur at rate ap/τ and are unconstrained, while hops in the direction to the EMM have a rate aq/τ and are constrained by a factor $1 - C_1$, i.e., the probability that the site $X = h_t - a$ is vacant at time t .

Consider now the evolution of $C(X,t)$ on sites X of the interval $[0, h_t - 2a]$. Particles that may be present at this interval all have equal probabilities of hops up and down and all are indistinguishable: the BP with its asymmetric transition rates is by definition at the site $X = h_t$. As a consequence, a forbidden attempt of any particle to hop onto the well already occupied by another particle is quite equivalent to the event when both simply interchange their positions, which means that hard-core exclusion is not very important (see also [48]) for the evolution of $C(X,t)$ on $[0, h_t - 2a]$. Thus, as a reasonably good approximation we suppose that on this interval the concentration $C(X,t)$ obeys a standard diffusion equation:

$$\frac{\partial C(X,t)}{\partial t} = D \frac{\partial^2 C(X,t)}{\partial X^2}, \quad D = \frac{a^2}{4\tau}. \quad (4)$$

Rigorous analysis of the influence of hard-core effects on particle dynamics in some similar problems, which supports the approximation in Eq. (4), may be found in [49].

Finally, dynamics of $C(X,t)$ at $X = h_t - a$, for which effects of the hard-core exclusion do matter because of the asymmetry induced by the BP, are governed by

$$a \frac{dC_1}{dt} = -D \left. \frac{\partial C(X,t)}{\partial X} \right|_{(X=h_t-a)} - C_1 \frac{dh_t}{dt}. \quad (5)$$

In Eq. (5) the first, gradient term accounts for exchanges of identical fluid particles between the sites $h_t - 2a$ and $h_t - a$. The second term describes the change in the mean occupation of the site $X = h_t - a$ due to the motion of the BP and is proportional to the negative of the product of the BP velocity, dh_t/dt , and of C_1 . Here, the multiplier dh_t/dt determines the rate at which the site adjacent to the BP becomes

vacant due to the motion of the BP. In turn, the factor C_1 , which is the mean occupation of the site adjacent to the boundary particle, accounts in a mean-field manner for the following circumstance: Suppose that at time t the BP is at h_t and the site $X = h_t - a$ is vacant, i.e., $\eta(X = h_t - a, t) = 0$. Then, if at the time moment $t + \tau$ the BP makes a hop away from the EMM, it “creates” a vacancy at the previously occupied site and thus $\eta(X = h_t - a, t + \tau) = 0$ still equals zero. Therefore, the occupation of this site is not effectively changed in the case when prior to the BP hop the left-hand side (lhs) adjacent site was vacant. Conversely, if at time t the lhs adjacent to the BP site is occupied, i.e., $\eta(X = h_t - a, t) = 1$, and the BP hops away from the EMM, one has that $\eta(X = h_t - a, t + \tau) = 0$, i.e., is changed from one to zero.

Thus we have a complete, coupled system of dynamical Eqs. (3) to (5) describing the time evolution of the particle concentration $C(X,t)$ and the mean displacement h_t of the boundary particle (extension of the film). Below we will analyze its solutions in two situations: when q is strictly greater than p (Sec. IV), which means that there is a nonzero effective surface force acting on the BP, and when $p = q = p_0$ (Sec. V), which corresponds to zero surface force. The latter case is appropriate to spreading of strongly volatile liquids or to the experimental situation described in [24].

IV. SOLUTIONS OF DYNAMICAL EQUATIONS IN THE PRESENCE OF AN EFFECTIVE SURFACE FORCE

In this section we consider first (subsection A) the analytical solutions of the dynamical equations (3) to (5) in the case when an effective surface force ($q > p$) favors motion of the BP towards the EMM. Here we will determine explicitly the growth law of the film’s length and mass. In subsection B we will analyze the details of the fine structure of the growing film, such as the concentration profile along the film and also the time evolution of the particle concentration and concentration gradient at the extremities of the film. In subsection C we will present the results of numerical simulations of the stochastic process, described in Sec. III and compare our analytical predictions against these numerical results. Finally, at the end of subsection C we will discuss some similar features between our analytical findings and observations made in numerical simulations of liquid drop spreading.

A. Mean displacement of the boundary particle and mass of particles in the film

In order to find the solution of coupled Eqs. (3)–(5) we first recall that Eq. (4), unconstrained by the boundary conditions, has a solution that is stationary in the scaled variable $Xt^{-1/2}$. Accordingly, we will base our approach to the solution of Eqs. (3) to (5) on the *a priori* assumption that h_t actually grows in time as \sqrt{t} and that the concentration profile $C(X,t)$ attains a stationary form in terms of a scaled variable ω , $\omega = (X + a)/h_t$. We note that, of course, the solution so obtained must be tested for consistency with the initial assumption. Consequently, such an approach will be self-consistent if we succeed to show that there exists a fi-

nite, constant prefactor in the dependence $h_t \sim \sqrt{t}$, for which Eqs. (3)–(5) are compatible. A more accurate approach and time-dependent corrections to the stationary solution will be discussed in Sec. V and the Appendix.

Rewriting Eq. (4) in terms of the above-defined scaled variable ω we have

$$\frac{d^2 C(\omega)}{d\omega^2} + A_m \omega \frac{dC(\omega)}{d\omega} = 0, \quad (6)$$

where the parameter A_m is given by

$$A_m = \frac{1}{2D} \frac{dh_t^2}{dt} \quad (7)$$

and is expected, in view of our assumption, to be a time-independent constant. To find A_m explicitly we will proceed as follows: We notice first that since $dh_t/dt \rightarrow 0$ when $t \rightarrow \infty$, Eq. (3) ensures that C_1 rapidly, at rate $|dC_1/dt| \ll dh_t/dt$, approaches a constant value \tilde{C}_1 , $\tilde{C}_1 = 1 - p/q$. Then, solving the differential Eq. (6) subject to the boundary conditions $C(\omega=0) = C_0$ and $C(\omega=1) = \tilde{C}_1$ we find that the appropriate stationary solution reads

$$C(\omega) = C_0 + (\tilde{C}_1 - C_0) \frac{\text{erf}(\omega \sqrt{A_m/2})}{\text{erf}(\sqrt{A_m/2})}, \quad (8)$$

where $\text{erf}(x)$ denotes the error function. Next, rewriting Eq. (5) in terms of the scaled variable ω and neglecting transient terms, we have

$$\left. \frac{D}{h_t} \frac{dC(\omega)}{d\omega} \right|_{\omega=1} = -\tilde{C}_1 \frac{dh_t}{dt}. \quad (9)$$

Now, the derivative of $C(\omega)$ with respect to ω , which enters Eq. (9), can be readily expressed from Eq. (8) through the parameters A_m , C_0 , and \tilde{C}_1 , which gives

$$\left. \frac{dC(\omega)}{d\omega} \right|_{\omega=1} = \sqrt{\frac{2A_m}{\pi}} \frac{(\tilde{C}_1 - C_0) \exp(-A_m/2)}{\text{erf}(\sqrt{A_m/2})}. \quad (10)$$

Plugging then Eq. (10) into Eq. (9) we arrive at the following equation:

$$\sqrt{\frac{2A_m}{\pi}} \frac{(\tilde{C}_1 - C_0) \exp(-A_m/2)}{\text{erf}(\sqrt{A_m/2})} = -\frac{\tilde{C}_1}{2D} \frac{dh_t^2}{dt}, \quad (11)$$

which, making use of the definition of parameters A_m and \tilde{C}_1 , can be cast into the form

$$\begin{aligned} \sqrt{\frac{\pi A_m}{2}} \exp\left(\frac{A_m}{2}\right) \text{erf}\left(\sqrt{\frac{A_m}{2}}\right) &= \frac{p - q + q C_0}{q - p} \\ &= \frac{1 - \exp[-\beta(E_\perp - W_\perp)]}{\exp(\beta W_\perp) - 1}, \end{aligned} \quad (12)$$

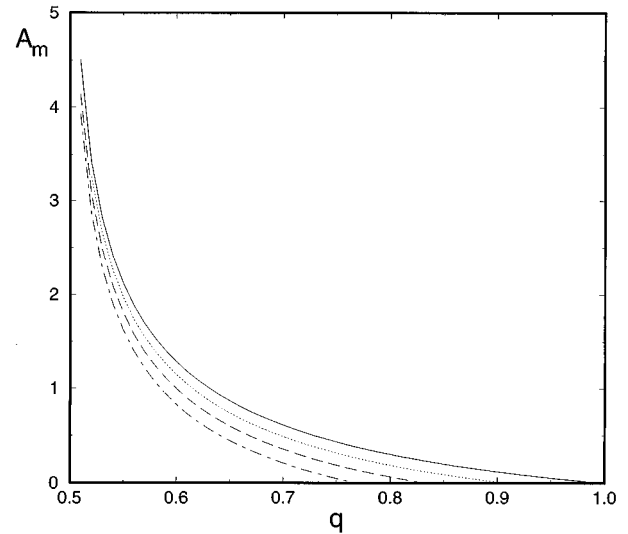


FIG. 4. The parameter A_m as a function of the transition probability q ($p+q=1$) at different values of the concentration at the edge of the macroscopic meniscus, C_0 . The upper curve (solid line) corresponds to $C_0=1$, the dotted line to $C_0=0.9$, the dashed line to $C_0=0.8$, and the dot-dashed line to $C_0=0.7$.

i.e., into the form of a closed with respect to A_m equation, which defines its dependence on the given parameters p , q , and C_0 (or E_\perp and W_{aj}).

Equation (12) shows thus that for any values of the parameters W_\perp and E_\perp (except for the case $p=q$, when $W_\perp=0$, which will be studied in Sec. V) the parameter A_m is actually a well-defined positive constant. Consequently, we may claim that the mean displacement of the boundary particle, or, in other words, the mean extension of the wetting film, obeys

$$h_t = \sqrt{2A_m D t}. \quad (13)$$

Equation (13) constitutes the primary result of our analysis and agrees with the experimentally observed behavior [6,13–15,22,23]. We note also that it may be somewhat misleading to call the behavior in Eq. (13) ‘‘diffusive’’; here it describes the growth of the *mean* displacement, which is exactly equal to zero for diffusive-type processes. Accordingly, the phenomenon of spreading of thin liquid films stems from essentially different processes than, say, growth of the area visited by an unconstrained random walk. Spreading of thin films is controlled merely by the transport of vacancies along the solid wall from the tip of the film to the macroscopic liquid edge, where these vacancies are filled by fluid particles, a behavior that is reminiscent, in view of underlying physical processes, of the phenomena of the directional solidification, melting or freezing, in which the spreading of the front of a ‘‘new’’ phase is controlled by the rate at which the particles of the ‘‘old’’ phase diffuse away of the front [50].

Now, in Fig. 4 we depict the numerical solution of Eq. (12), which represents A_m as a function of the transition probability q at four different values of the concentration C_0 . This figure shows that for q sufficiently close to $1/2$ (we took $p+q=1$) A_m is large (it diverges when q is exactly equal

1/2) and its magnitude is not very sensitive to the actual value of the concentration at the EMM, C_0 . At greater q the parameter A_m tends to zero and becomes equal to zero at finite values of q , which depend on the concentration C_0 . This critical value can be readily estimated from Eq. (12). Namely, it may be obtained by equating the right-hand side (rhs) of Eq. (12) to zero, which yields $p_c/q_c = 1 - C_0$. The latter equation means that $A_m = 0$ (no spreading) when the probability of hops away from the EMM is equal to the probability of hops towards the EMM times the mean occupation of the left-hand adjacent site.

Now, we estimate analytically the dependence of A_m on the pertinent parameters in the asymptotic limit when A_m is small or large. It follows from Eq. (12) that A_m is small when the rhs of Eq. (12) is small. It happens, namely, when $p \approx q(1 - C_0)$. In terms of the energetic parameters E_{\downarrow} and W_{\leftarrow} it means that A_m is small when either the inequality $\beta E_{\downarrow} > \beta W_{\leftarrow} \gg 1$ holds (what may be thought of as the case of liquids with high cohesion energy and strong attraction to the substrate), or when the difference

$$s = E_{\downarrow} - W_{\leftarrow} \quad (14)$$

is sufficiently small, such that $\beta s \ll \exp(\beta W_{\leftarrow}) - 1$. When either of these inequalities is fulfilled A_m is given explicitly by

$$A_m \approx \frac{p - q + qC_0}{q - p}, \quad (15)$$

which, using the energetic parameters, can be rewritten as

$$A_m \approx \frac{1 - \exp(-\beta s)}{\exp(\beta W_{\leftarrow}) - 1}. \quad (16)$$

We note now that the growth of the film occurs as long as the parameter s , Eq. (14), is positive. Therefore, it seems natural to define s as the *microscopic* analog of the spreading parameter S —the property that is the key parameter determining spreading of liquids at the macroscopic scales [1–5]. Explicitly, S is the free energy difference between a bare solid, directly in contact with the vapor and a solid covered by a flat, thick liquid layer and thus compares the surface tensions of three different interfaces involved when a liquid drop is deposited on a solid substrate. For $S > 0$ the drop spontaneously spreads and tends to shield the substrate. In the case when S is negative the liquid remains in the form of a droplet. In our situation with spreading of a molecularly thin film, the parameter s , which equals the difference of the energy gained by filling by a fluid particle a vacancy at the EMM and the work required to transport a vacancy from the tip of film to the EMM, is the key parameter that distinguishes whether the monolayer will grow or not. Consequently, we will call it the *microscopic* spreading parameter.

Now, A_m may be large when the rhs of Eq. (12) is large, which happens in the situations when p is very close to (but less than) q . In terms of the energetic parameters this corresponds to the case when $\beta W_{\leftarrow} \ll 1$, provided that s is sufficiently large. In this case A_m reads

$$A_m \approx 2 \ln \left[\frac{\sqrt{2}(p - q + qC_0)}{\sqrt{\pi}(q - p)} \right], \quad (17)$$

or, in terms of E_{\downarrow} and W_{\leftarrow} ,

$$A_m \approx 2 \ln \left[\frac{\sqrt{2}[1 - \exp(-\beta s)]}{\sqrt{\pi}[\exp(\beta W_{\leftarrow}) - 1]} \right]. \quad (18)$$

Behavior as in Eqs. (17) and (18) may be realized experimentally in the case of liquids with low cohesion energy, which are volatile in two dimensions, but not volatile in three dimensions. An example of such a liquid is squalane (see [14] for details).

Finally, we examine the evolution of the mass M_t of the film, which is defined by

$$M_t = \int_{-a}^{h_t - a} dX C(X, t). \quad (19)$$

Changing the variable of integration and making use of Eq. (8) we get

$$M_t = h_t \int_0^1 d\omega C(\omega) = h_t \exp(A_m/2) [1 - \exp(-\beta W_{\leftarrow})], \quad (20)$$

which shows that M_t also grows in proportion to \sqrt{t} , in accord with experimental observations [13,51].

A remarkable feature of the result in Eq. (20) is that the mean particle concentration ρ , $\rho = M_t/h_t = \exp(A_m/2)[1 - \exp(-\beta W_{\leftarrow})]$, turns out to be time independent. In the case of small A_m the mean particle concentration is close to unity, while for progressively large A_m it tends to zero. This behavior is illustrated in Fig. 8, where we plot the functions M_t/\sqrt{t} , h_t/\sqrt{t} , and ρ versus the transition probability q .

B. Fine structure of the film

Consider the concentration profiles defined by Eq. (8). In Fig. 5 we plot the particle concentration for several different values of the parameter A_m ; in Fig. 5(a) it is plotted versus the scaled variable ω and in Fig. 5(b) versus the variable X (for a fixed moment of time $t = 10^3 \tau$). Figure 5 shows that the shape of the curve describing the stationary concentration profile is rather sensitive to the value of A_m (and, in turn, to the values of the parameters W_{\leftarrow} and E_{\downarrow}). When A_m is small enough (the dotted and the solid lines in Fig. 5 correspond to $A_m \approx 0.565$ and $A_m \approx 1.067$, respectively) the profiles $C(\omega)$ and $C(X)$ are almost linear. In this limit the error function in Eq. (8) can be expanded in powers of $\sqrt{A_m}$ and already the first term in this expansion provides a fairly nice estimate for the entire interval on which ω or X are defined. When A_m exceeds unity this is no longer so and the shape of the profile becomes quite different. In Fig. 5 the dash-dotted line corresponds to $A_m \approx 3.089$ and the dashed line to $A_m \approx 6.843$. From the viewpoint of the relevance to experimental situations, the first two curves (with low values of A_m) correspond to nonvolatile liquids, i.e., such that βW_{\leftarrow} is large and evaporation of particles out of the liquid phase into the vapor is suppressed. Two other profiles, in contrast, are appropriate to situations with volatile liquids, for which the cohesion energy is low and particles easily evaporate into the vapor phase.

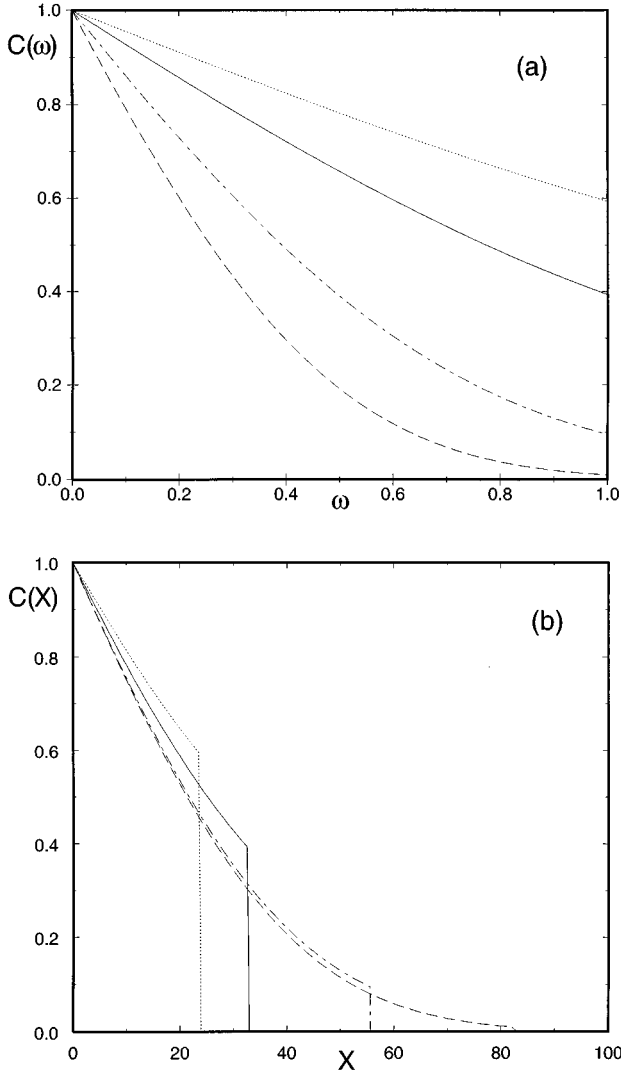


FIG. 5. The particle concentration profiles in the growing film. We plot in (a) the function $C(\omega)$, Eq. (8), vs the variable ω for different values of the parameter βW_+ and fixed $\beta s=5$. In (b) we depict the profiles $C(X,t)$ vs the variable X at a fixed moment of time $2Dt=10^3$ and different values of the energetic parameters. In both (a) and (b) the upper curve (dotted line) corresponds to $\beta W_+=0.9$ ($A_m=0.565$), the solid line to $\beta W_+=0.5$ ($A_m=1.067$), the dash-dotted line to $\beta W_+=0.1$ ($A_m=3.089$), and the dashed line gives the variation of the profile for $\beta W_+=0.01$ ($A_m=6.843$).

Next, we consider time evolution of C_1 and of the concentration gradients at the extremities of the growing film. Eqs. (3) and (13) give

$$C_1 = 1 - \frac{p}{q} + \frac{\tau}{aq} \frac{dh_t}{dt} \approx [1 - \exp(-\beta W_+)] \left[1 + \coth(\beta W_+/2) \sqrt{\frac{A_m \tau}{2t}} \right]. \quad (21)$$

The behavior of the derivatives of the stationary concentration profile at points $\omega=0$ and $\omega=1$ can be readily found from Eq. (8) and read

$$\left. \frac{dC(\omega)}{d\omega} \right|_{\omega=1} = -\tilde{C}_1 A_m \quad (22)$$

and

$$\left. \frac{dC(\omega)}{d\omega} \right|_{\omega=0} = -\tilde{C}_1 A_m \exp(A_m/2), \quad (23)$$

which shows that the current of particles away from (or the current of vacancies to) the EMM is a factor of $\exp(A_m/2)$ greater than the current of particles at the tip of the film. Rewriting the results in Eqs. (22) and (23) in terms of variables X and t we have, respectively,

$$\left. \frac{\partial C(X,t)}{\partial X} \right|_{X=h_t-a} = -\tilde{C}_1 \sqrt{\frac{A_m}{2Dt}}, \quad (24)$$

$$\left. \frac{\partial C(X,t)}{\partial X} \right|_{X=-a} = -\tilde{C}_1 \sqrt{\frac{A_m \exp(A_m)}{2Dt}}, \quad (25)$$

i.e., the concentration gradients at both extremities of the film decrease in time in proportion to $1/\sqrt{t}$.

From Eqs. (21) to (25) we infer that relaxation processes in the film proceed fundamentally more slowly than these in the macroscopic liquid; relaxation of concentrations to their equilibrium values is described by a power-law.

C. Numerical simulations

In this subsection we check the results of our mean-field continuous-space and time description of the discrete space and time stochastic process defined in Sec. III against the results of numerical Monte Carlo simulation of this process. The simulation algorithm and the results will be presented in the beginning of this section. At the end of this section we will also present the qualitative comparison of our analytical results and the results of numerical simulations of liquid drop spreading, performed in [31].

The simulation algorithm follows the definition of the stochastic process closely, except that to shorten the simulation time we stipulate that neither particle can choose to remain at its position, i.e., $p+q=1$ for the boundary particle and all other particles select the direction of jump with probability 1/2. Additionally, we set the ‘‘stick’’ time $\tau=1$ and also $a=1$, which means that the diffusion constant $D=1/2$. More precisely, we consider a segment (Fig. 3) of a one-dimensional regular lattice of unit spacing with sites $X=-1, 0, \dots, L$, where L is taken to be sufficiently large to avoid finite-size effects. At the Monte Carlo (MC) time moment $\Delta_0=0$ we land two particles at the sites $X=-1$ and $X=0$. At $\Delta_1=1$ one of these particles is chosen at random and is allowed to perform a hop. If the chosen particle is the one at $X=-1$, it attempts to hop to the right with probability 1/2, or, with the probability 1/2 remains at its position. In this initial configuration, however, the hop to the right cannot be fulfilled because at this moment of the MC time the particle at $X=-1$ is blocked by the particle at $X=0$. Now, if the chosen particle is the one at $X=0$ (the boundary particle), it first selects the direction of hop with the probability q for hops to the left and the probability p for hops to the right. As

we have already noted, we took here $p + q = 1$, which means that the choice should be made strictly between the right and left—the probability to remain at its position is zero. If the selected direction is to the right, the hop is fulfilled and the particle jumps onto the site $X=1$ and creates a “vacancy” at $X=0$. Otherwise, it remains at $X=0$ and at the next moment of the MC time the procedure is repeated. Eventually, the particle at $X=-1$ performs a hop onto the site $X=0$ and makes the site $X=-1$ vacant. When this happens a new particle lands on the site $X=-1$, which means that at the site $X=-1$ we introduce a source, which keeps the occupation of this site fixed. For simplicity, we stipulate that the source lands a particle onto this site as soon as it becomes vacant, which means that $C_0=1$ ($\beta E_{\downarrow} \gg 1$) at any moment of time. Now, the rules are essentially the same when three or more particles are present on the lattice. At each moment of the MC time one particle among all is chosen at random. If the chosen particle is not the particle at $X=-1$ and is not the boundary, the rightmost particle, then it selects the direction of hop with equal probabilities ($1/2$) for hops to the right and to the left. The jump is instantaneously fulfilled if the neighboring site in the selected direction is vacant. If the chosen particle is the boundary one, the probability of hopping to the right is p , while that for the hopping to the left is q . For the BP the jump to the left is constrained by hard-core interactions with the adjacent particle, while hops to the right are instantaneously fulfilled provided that this direction is selected. Finally, for the particle at $X=-1$ the probability of hopping to the right is $1/2$ and it may remain, with probability $1/2$, at $X=-1$.

In simulations the time evolution of several different properties was measured. We have recorded the mean displacement of the boundary particle, the number of particles (mass) on the lattice at time t , concentration profiles and the concentration at the site adjacent to the position of the boundary particle. Each realization of the process started at the initial configuration with two particles and was terminated when there were 400 particles on the lattice. Care has been taken that for neither realization does the boundary particle reach the system’s boundary L .

Results of our simulations are presented in Figs. 6–8 and the time evolution of the properties under study is plotted versus the real physical time. This time is defined in a standard fashion for the MC simulations of systems with a variable number of particles; while the MC time varies continuously, the real time is increased by a fixed unit value only when a number of particles on the line gets increased. In other words, the step of physical time Δt is related to Δ_n as $\Delta t = \Delta_n / M_n$, where M_n is the number of particles on the lattice at the MC moment Δ_n .

In Fig. 6 we plot our analytical, Eq. (13) with $D=1/2$, and numerical results for the length of the film at four different values of the transition probability q ($q=0.6, 0.7, 0.8$, and 0.9) versus \sqrt{t} . For such values of parameters numerical simulations give, respectively, the following values of the parameter A_m : $A_m=1.277, 0.613, 0.298$, and 0.121 . From Eq. (12) we have the corresponding analytical results for A_m , which are $A_m=1.282, 0.609, 0.301$, and 0.120 . The maximal discrepancy between our analytical and numerical results occurs for $q=0.7$, but amounts, however, to less than 1%.

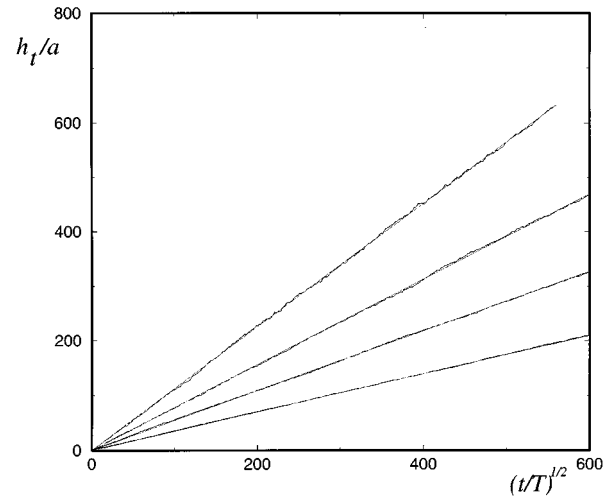


FIG. 6. Length of the film vs \sqrt{t} at different values of q and fixed $C_0=1$. The upper curve (solid line) gives the analytical result for $q=0.6$. The noisy line represents the data of numerical simulations. Other curves are the corresponding analytical and numerical results for $q=0.7, 0.8$, and 0.9 , respectively.

In Fig. 7 we plot our analytical, Eq. (20), and numerical results for the growth of the mass of the film versus \sqrt{t} . Agreement between the theoretical predictions for this property and numerical data is here even better and the error is considerably less than 1%; in fact, the analytical and numerical curves are almost indistinguishable. Finally, Fig. 8 shows the analytical curves h_t/\sqrt{t} , M_t/\sqrt{t} , and mean concentration ρ as functions of the transition probability q . Diamonds and crosses in this figure show the corresponding values of the prefactors in the time dependences of h_t and M_t deduced from the numerical data. Again, the agreement between our analytical predictions and numerical data is quite good.

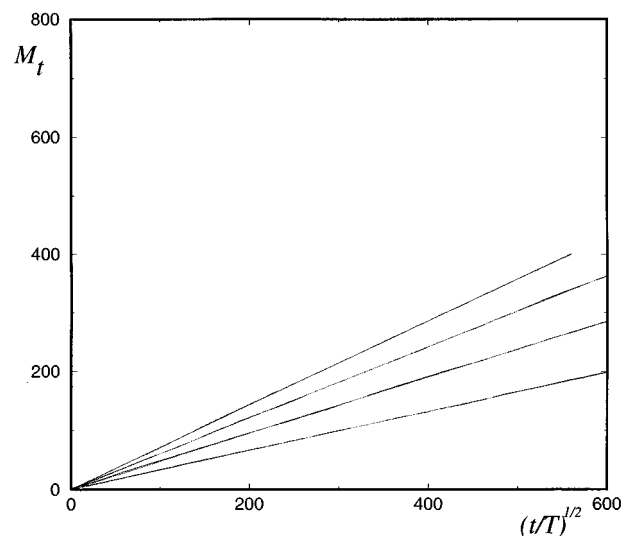


FIG. 7. Mass of the film vs \sqrt{t} . The upper solid line corresponds to $q=0.6$. The curves in order from up to down are the results for $q=0.7, 0.8$, and 0.9 , respectively.

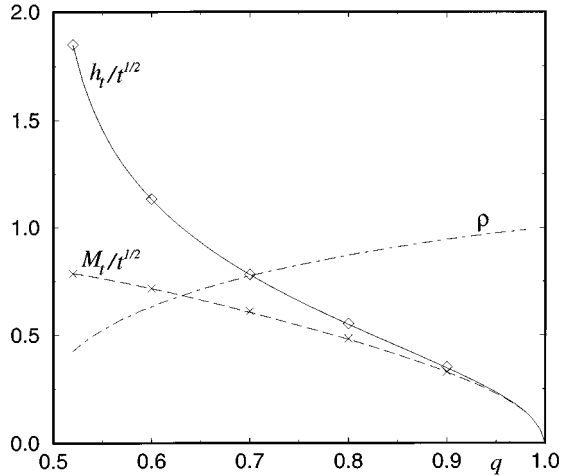


FIG. 8. Plot of the functions h_t/\sqrt{t} (solid line), M_t/\sqrt{t} (dashed line), and mean concentration ρ (dot-dashed line) vs the transition probability q . Open diamonds and crosses give the numerical data.

To close this section we present a succinct qualitative comparison of our analytical results with the results of numerical simulations performed in [31], which also employed a very similar lattice-gas picture of the spreading phenomena. In this model the hard-core particles, initially placed in a volume with a ridgelike shape, perform random motion prescribed by the Kawasaki spin-exchange dynamics (see for more details [31]). The interactions involved are hard core at the molecular size, interactions with nearest neighbors via the coupling constant J , which describes cohesion between fluid particles, and also attractive van der Waals interactions, $V(z) = -A/z^2$, with the substrate; z is the distance from the substrate and A is the Hamaker constant. In [31] behavior of h_t was analyzed as a function of parameters βJ and A/J . One of the most interesting observations made was that, at a fixed βJ , the substantial change in the substrate potential strength does not affect the behavior of h_t very dramatically. For instance, for $\beta J = 1/2$ the increase in A/J from 5 to 100 caused the precursor length to differ only less than 10% after 150 000 time steps. Now, noticing that parameters J and A in [31] are qualitatively the same as our W_{\perp} and E_{\perp} let us see how the change of their magnitude affects the growth of the film, Eq. (13). In Fig. 9 we plot the parameter A_m as a function of the *microscopic* spreading parameter for several different values of βW_{\perp} : $\beta W_{\perp} = 0.1, 0.5$, and 0.9 . We show that also in our model the value of A_m , at a fixed βW_{\perp} , does not vary significantly with a strong variation of the spreading parameter s . For instance, taking $\beta W_{\perp} = 1/2$ and $\beta s = 5$ we find from Eq. (12) that $A_m \approx 1.062$ while increasing βs up to 100 we have $A_m \approx 1.067$, i.e., the value that is only 0.5% off. Consequently, our analytical results show that the change in the value of βs from 5 to 100 will make the film's length larger in only less than 7%. Finally, let us remark that the situation is reminiscent of that with the macroscopic spreading parameter S ; although spreading of a droplet at the macroscopic scales occurs only as S is positive, the rate of growth of the macroscopic liquid edge is weakly, logarithmically dependent on the actual value of S [1–12].

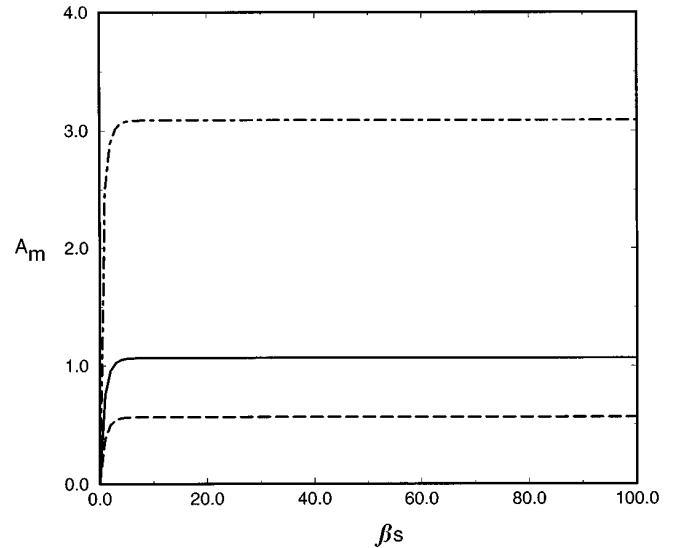


FIG. 9. The parameter A_m as the function of the microscopic spreading parameter βs . The upper curve (the dash-dotted line) corresponds to $\beta W_{\perp} = 0.1$, the solid line to $\beta W_{\perp} = 0.5$, and the dashed line to $\beta W_{\perp} = 0.9$.

V. SOLUTIONS OF DYNAMICAL EQUATIONS IN THE ABSENCE OF AN EFFECTIVE SURFACE FORCE

To complete our presentation we consider the spreading kinetics and the fine structure details of growing films in the special case $p = q$ when an effective surface force is absent. This case is relevant to liquids with very low cohesion energy, i.e., strongly volatile liquids. We hasten to remark that our present model does not include the possibility of particle evaporation in the direction normal to the solid wall, which may take place in experiments with volatile liquids. However, the possibility of the evaporation along the wall, i.e., two-dimensional evaporation, is well captured by our model. Therefore, in the following we will assume that βE_{\perp} is sufficiently large and the evaporation normal to the solid wall is suppressed; i.e., we will constrain ourselves to experimental situations for which our model makes sense.

We notice also that the situation with zero surface force is appropriate to the experimental situation discussed in [24], which was concerned with spreading of metallic beads and the setup of which we depict in Fig. 10. Here a horizontal

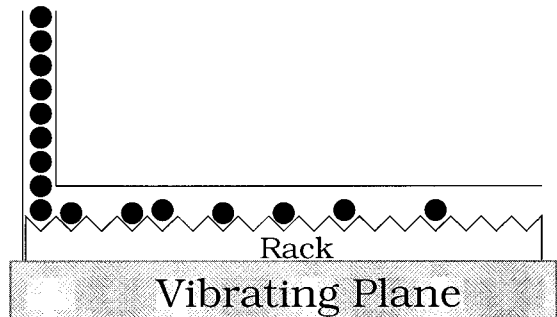


FIG. 10. Experimental setup of Ref. [24]. Spreading of metallic beads on a vibrating racklike corrugated plane.

rack, confined inside of a rectangular tube, is fixed on a plane. A vertical stack is placed at the left end of the rack. The plane is vibrated by two motors, whose flywheels are eccentric and produce irregular (chaotic) vibrations. Now, a column of metallic beads is introduced into the stack and, as soon as the vibration is switched on, the beads start to move along the rack away from the stack. The size of the beads is chosen in such a way that only a single bead can occupy a given slot of the rack. In addition, the distance between the top of the slot and the top of the tube only slightly exceeds the radius of bead. Consequently, the beads cannot pass through each other. In this experiment both the mean (over several realizations) displacement of the rightmost bead and the mean number (or mass) of beads on the rack are found to grow in proportion to \sqrt{t} [24].

We turn now to the behavior of Eqs. (3) to (5) in the case when all particles including the BP have equal probabilities for jumps to the right and to the left, $p=q=p_0$. Diffusion coefficient in this case will be $D=a^2p_0/\tau$.

We recall first that as we have seen in Sec. IV this case is somewhat peculiar since the rhs of Eq. (12) diverges, which means that A_m is no longer a well-defined constant but rather is some increasing function of time. Equation (17) shows that when q tends to p the divergence in A_m is logarithmic, i.e., $A_m \propto -\ln|q-p|$. Therefore, one may expect (and this will be shown to be the case) that in the case $q=p$ the parameter A_m should grow in time as a logarithm of t . Consequently, the approach devised in the previous section cannot be directly applied here since one cannot *a priori* claim the existence of the stationary solution in Eq. (8). However, as we proceed to show, even in this case Eq. (8) represents a fair approximation of $C(X,t)$ when time t is sufficiently large.

We start our analytical analysis by noticing that the solution of diffusion Eq. (4) with the boundary conditions $C(X=-a,t)=C_0$ and $C(X=h_t-a,t)=C_1(t)$ can be written in the following general form:

$$C(X,t)=\bar{C}(\omega,t,C_1). \quad (26)$$

Consequently, the derivatives of $C(X,t)$ with respect to the time and space variables will read

$$\frac{\partial C(X,t)}{\partial t} = -\frac{\omega}{h_t} \frac{dh_t}{dt} \frac{\partial \bar{C}}{\partial \omega} + \frac{\partial \bar{C}}{\partial t} + \frac{\partial \bar{C}}{\partial C_1} \frac{dC_1}{dt}, \quad (27)$$

$$\frac{\partial^2 C(X,t)}{\partial X^2} = \frac{1}{h_t^2} \frac{\partial^2 \bar{C}}{\partial \omega^2}, \quad (28)$$

and Eq. (4) will take the form

$$\frac{\partial^2 \bar{C}}{\partial \omega^2} + A_m \omega \frac{\partial \bar{C}}{\partial \omega} = \frac{h_t^2}{D} \left[\frac{\partial \bar{C}}{\partial t} + \frac{\partial \bar{C}}{\partial C_1} \frac{dC_1}{dt} \right], \quad (29)$$

which is to be solved subject to the boundary conditions

$$\bar{C}(\omega=0,t,C_1)=C_0, \quad \bar{C}(\omega=1,t,C_1)=C_1. \quad (30)$$

Now, we will seek the solution of Eqs. (29) and (30) as an expansion in the powers of inverse diffusion coefficient, i.e.,

$$\bar{C}(\omega,t,C_1) = \sum_{n=0}^{\infty} D^{-n} \Psi_n(\omega,t,C_1), \quad (31)$$

in which $\Psi_0(\omega,t,C_1)$ obeys Eq. (6) with the boundary conditions $\Psi_0(\omega=0,t,C_1)=C_0$ and $\Psi_0(\omega=1,t,C_1)=C_1$ and thus is given explicitly by Eq. (8). The higher-order terms, i.e., $\Psi_{n>0}(\omega,t,C_1)$, may be calculated recursively from equations

$$\frac{\partial^2 \Psi_n}{\partial \omega^2} + A_m \omega \frac{\partial \Psi_n}{\partial \omega} = h_t^2 \left[\frac{\partial \Psi_{n-1}}{\partial t} + \frac{\partial \Psi_{n-1}}{\partial C_1} \frac{dC_1}{dt} \right] \quad (32)$$

and

$$\Psi_n(\omega=0,t,C_1)=0, \quad \Psi_n(\omega=1,t,C_1)=0. \quad (33)$$

Next, to define the time evolution of A_m and h_t we will proceed as follows. Noticing that in the case $p=q=p_0$ Eq. (3) reduces to

$$C_1 = \frac{a}{D} \frac{dh_t}{dt} \quad (34)$$

we may rewrite Eq. (5) as

$$\frac{ah_t}{D^2} \left(\frac{dh_t}{dt} \right)^2 = - \frac{\partial \bar{C}}{\partial \omega} \Big|_{\omega=1} = - \sum_{n=0}^{\infty} D^{-n} \frac{\partial \Psi_n}{\partial \omega} \Big|_{\omega=1}. \quad (35)$$

Further on, assuming (the validity of this assumption will be checked in the Appendix) that

$$\left| \frac{\partial \Psi_0}{\partial \omega} \Big|_{\omega=1} \right| \gg \frac{1}{D^n} \left| \frac{\partial \Psi_n}{\partial \omega} \Big|_{\omega=1} \right| \quad (36)$$

we will neglect in the rhs of Eq. (35) all terms with $n>0$. Then, combining Eqs. (35) and (10) we will obtain

$$\frac{ah_t}{D^2} \left(\frac{dh_t}{dt} \right)^2 = \sqrt{\frac{2A_m}{\pi}} \frac{C_0 \exp(-A_m/2)}{\operatorname{erf}(\sqrt{A_m/2})}, \quad (37)$$

which, employing the definition of the parameter A_m , Eq. (7), can be cast in the following form:

$$A_m^{3/2} \exp(A_m/2) \operatorname{erf}(\sqrt{A_m/2}) = \sqrt{\frac{2}{\pi}} \frac{C_0 h_t}{a}. \quad (38)$$

We note now that the rhs of Eq. (38) diverges as $t \rightarrow \infty$ since h_t evidently grows with time. This means, in turn, that at sufficiently large times the dominant multiplier on the lhs of Eq. (38) is the exponent of $A_m/2$; the multiplier $A_m^{3/2}$ grows essentially slower and $\operatorname{erf}(\sqrt{A_m/2})$ is bounded by unity. Consequently, for the leading in time term in A_m we get

$$A_m \approx \ln \left(\frac{4C_0^2 D t}{\pi a^2} \right), \quad (39)$$

i.e., an expected logarithmic growth of A_m in time. Accordingly, the growth of the film's length in this case will obey

$$h_t \approx \sqrt{2Dt \ln\left(\frac{4C_0^2Dt}{\pi a^2}\right)}. \quad (40)$$

We hasten to remark that Eqs. (40) and (39) are asymptotic results and the time needed to ensure their utility may be considerably large. In [24], in which measurements were performed within a rather short time interval, the additional logarithmic factor has not been seen. We also doubt whether the slowly varying logarithmic multiplier can be distinguished in laboratory experiments with spreading of volatile liquids.

Consider now the time evolution of other characteristic properties of the film, such as the mass of particles, the mean concentration, and the concentration gradients. For the mass of particles we have from Eq. (20) (which is an exact equation for this property and holds also for the case $p=q=p_0$) that it grows as

$$M_t \approx C_0 \sqrt{\frac{4Dt}{\pi}}, \quad (41)$$

i.e., the additional logarithmic multiplier does not appear and the mass of particles grows in proportion to \sqrt{t} . Accordingly, from Eqs. (40) and (41), we find that the mean concentration ρ slowly decreases with time:

$$\rho \approx C_0 \sqrt{\frac{2}{\pi \ln(4C_0^2Dt/\pi a^2)}}. \quad (42)$$

The particle concentration on the left-hand side adjacent to the BP site may be readily found from Eqs. (34) and (40) and obeys

$$C_1 \approx \left(\frac{a^2}{2Dt}\right)^{1/2} \ln^{1/2}\left(\frac{4C_0^2Dt}{\pi a^2}\right). \quad (43)$$

Finally, for the concentration gradient at the point $\omega=0$ (and $X=-a$) we have

$$\left.\frac{\partial C(\omega)}{\partial \omega}\right|_{\omega=0} \approx -C_0 \sqrt{\frac{2}{\pi} \ln\left(\frac{4C_0^2Dt}{\pi a^2}\right)} \quad (44)$$

and

$$\left.\frac{\partial C(X,t)}{\partial X}\right|_{X=-a} \approx -\frac{C_0}{\sqrt{\pi Dt}}, \quad (45)$$

while the gradient at the point $\omega=1$ (and $X=h_t-a$) obeys

$$\left.\frac{\partial C(\omega)}{\partial \omega}\right|_{\omega=1} \approx -C_1 A_m \approx -\left(\frac{a^2}{2Dt}\right)^{1/2} \ln^{3/2}\left(\frac{4C_0^2Dt}{\pi a^2}\right) \quad (46)$$

and

$$\left.\frac{\partial C(X,t)}{\partial X}\right|_{X=h_t-a} \approx -\frac{a}{2Dt} \ln\left(\frac{4C_0^2Dt}{\pi a^2}\right). \quad (47)$$

VI. CONCLUSIONS

To summarize, we have presented a microscopic, molecular model describing the growth of monomolecularly thin liquid films in systems with planar (capillary rise) geometry. We have found analytically that both the length and the mass (number of particles) of the film grow in proportion to \sqrt{t} , in accord with the experimentally observed behaviors. The prefactors in this law are determined analytically and in two limiting cases explicit expressions are derived. We have determined a microscopic parameter that determines the physical conditions when the growth of films occurs and also analyzed the underlying physical mechanism of the film growth. We show that the essential physical process responsible for such a growth is associated with the diffusive transport of vacancies from the tip of the film to the edge of the macroscopic meniscus, where they are filled with fluid particles. In addition, we have examined the time evolution of several characteristic properties, which define the fine structure of the film. These are the mean concentration, concentration profiles along the film length, the particle concentration at the tip of the film, and also the concentration gradients. Numerical simulations are in a very good agreement with our analytical predictions for both the time evolution and the values of the prefactors for different parameters of the model.

ACKNOWLEDGMENTS

The authors thank M. Robbins and S. Granick for helpful discussions. We are also very grateful to J. L. Lebowitz for numerous discussions on the hard-core lattice gases dynamics. S.F.B. acknowledges a partial support by the ONR Grant No. 00014-94-1-0647 and from the University of Paris VI. G.O. acknowledges financial support from the CNRS.

APPENDIX

In this Appendix we consider the behavior of $\partial\Psi_1/\partial\omega$ and check our assumption that corrections to the stationary solution in Eq. (8) are insignificant at large times, provided that the parameter A_m is either a constant or a slowly varying in time function. From Eqs. (32) and (33) one may readily derive the first correction term, which is given explicitly by

$$\Psi_1 = \sqrt{\frac{2A_m}{\pi}} \frac{h_t^2}{\text{erf}(\sqrt{A_m/2})} \int_0^\omega d\omega_1 \int_0^1 d\omega_2 \int_{\omega_2}^{\omega_1} d\omega_3 \exp\left(-\frac{A_m}{2}(\omega_1^2 + \omega_2^2 - \omega_3^2)\right) \left(\frac{\partial}{\partial t} + \frac{dC_1}{dt} \frac{\partial}{\partial C_1}\right) \Psi_0. \quad (A1)$$

Now, the analysis of the exact form as in Eq. (A1) seems rather cumbersome, and we will merely try to find an upper bound on the absolute value of this function. To do this, we first note that

$$\left| \left(\frac{\partial}{\partial t} + \frac{dC_1}{dt} \frac{\partial}{\partial C_1} \right) \Psi_0 \right| \leq \frac{a}{D} \left| \frac{d^2 h_t}{dt^2} \right|. \quad (\text{A2})$$

Employing the inequality in Eq. (A2) we may bound $|\Psi_1|$ from above by

$$|\Psi_1| \leq \sqrt{\frac{2A_m}{\pi}} \frac{ah_t^2}{D \operatorname{erf}(\sqrt{A_m/2})} \left| \frac{d^2 h_t}{dt^2} \right| \int_0^\omega d\omega_1 \int_0^1 d\omega_2 \int_0^{\omega_1} d\omega_3 \exp\left(-\frac{A_m}{2}(\omega_1^2 + \omega_2^2 - \omega_3^2)\right) \leq \frac{\pi^{1/2} ah_t^2}{DA_m} \left| \frac{d^2 h_t}{dt^2} \right| \operatorname{erf}(\omega \sqrt{A_m/2}). \quad (\text{A3})$$

Consequently, we will obtain from (A3) that

$$\left| \frac{\partial \Psi_1}{\partial \omega} \right|_{\omega=1} \leq \frac{ah_t^2 \exp(-A_m/2)}{D \sqrt{A_m}} \left| \frac{d^2 h_t}{dt^2} \right|. \quad (\text{A4})$$

Now, in the case $q > p$ the derivative $\partial \Psi_0 / \partial \omega$ at point $\omega=1$ assumes constant values $-(1-p/q)A_m$, Eq. (22),

while $\partial \Psi_0 / \partial \omega$ at point $\omega=1$ is bounded from above, Eq. (A4), by a function that tends to zero as $1/\sqrt{t}$ when $t \rightarrow \infty$. In the case $p=q$ the derivative $\Psi_0 / \partial \omega$ at point $\omega=1$ vanishes as $\ln^2(t)/\sqrt{t}$ when $t \rightarrow \infty$, while the derivative of Ψ_1 is bounded by a function that decreases as $\ln^{1/2}(t)/t^{3/2}$. We thus may infer that in both cases at sufficiently large times Ψ_0 [and thus the stationary solution in Eq. (8)] represents the leading term in the expansion in Eq. (31).

-
- [1] P. G. de Gennes, *Rev. Mod. Phys.* **57**, 827 (1985).
[2] A. M. Cazabat, *Contemp. Phys.* **28**, 347 (1987).
[3] P. Ball, *Nature (London)* **337**, 624 (1989).
[4] L. Léger and J. F. Joanny, *Rep. Prog. Phys.* **72**, 431 (1992).
[5] M. L. Forcada and C. M. Mate, *Nature (London)* **363**, 527 (1993).
[6] A. M. Cazabat and M. A. Cohen Stuart, *J. Phys. Chem.* **90**, 5845 (1986).
[7] L. H. Tanner, *J. Phys. D* **12**, 1478 (1979).
[8] J. F. Joanny and P. G. de Gennes, *J. Phys. (Paris)* **47**, 121 (1986).
[9] F. Brochard, *J. Chem. Phys.* **84**, 4664 (1986).
[10] F. Brochard-Wyart, P. G. de Gennes, and H. Hervet, *Adv. Colloid Interface Sci.* **34**, 561 (1991).
[11] D. Ausserré, A. M. Picard, and L. Léger, *Phys. Rev. Lett.* **57**, 2671 (1986).
[12] L. Léger *et al.*, *Phys. Rev. Lett.* **60**, 2390 (1988).
[13] F. Heslot, N. Fraysse, and A. M. Cazabat, *Nature (London)* **338**, 640 (1989).
[14] F. Heslot, A. M. Cazabat, and P. Levinson, *Phys. Rev. Lett.* **62**, 1286 (1989).
[15] F. Heslot, A. M. Cazabat, P. Levinson, and N. Fraysse, *Phys. Rev. Lett.* **65**, 599 (1990).
[16] K. Kaski, *Europhys. News* **26**, 23 (1995).
[17] W. B. Hardy, *Philos. Mag.* **38**, 49 (1919).
[18] F. Tiberg and A. M. Cazabat, *Europhys. Lett.* **25**, 205 (1994).
[19] A. M. Cazabat, J. De Coninck, S. Hoorelbeke, M. P. Valignat, and S. Villette, *Phys. Rev. E* **49**, 4149 (1994).
[20] J. De Coninck, S. Hoorelbeke, M. P. Valignat, and A. M. Cazabat, *Phys. Rev. E* **48**, 4549 (1993).
[21] A. M. Cazabat, *Adv. Colloid Interface Sci.* **34**, 73 (1991).
[22] F. Heslot, A. M. Cazabat, and N. Fraysse, *J. Phys. Condens. Matter* **1**, 5793 (1989).
[23] A. M. Cazabat, N. Fraysse, and F. Heslot, *Colloids Surf.* **52**, 1 (1991).
[24] S. F. Burlatsky, J. G. Berberian, J. Shore, and W. P. Reinhardt, *Phys. Rev. E* **54**, 1489 (1996).
[25] J. A. Nieminen, D. B. Abraham, M. Karttunen, and K. Kaski, *Phys. Rev. Lett.* **69**, 124 (1992).
[26] J.-x. Yang, J. Koplik, and J. R. Banavar, *Phys. Rev. Lett.* **67**, 3539 (1991).
[27] J.-x. Yang, J. Koplik, and J. R. Banavar, *Phys. Rev. A* **46**, 7738 (1992).
[28] The authors of [26,27] discuss in detail the possible origin of the discrepancy between their numerical findings and the behavior observed in laboratory experiments [13–15]. Several different reasons are mentioned including comparatively small number of molecules in the simulation, the fact that simulations were conducted at thermodynamic conditions not far from the freezing temperature, cutoff of the liquid-solid interactions at a fixed distance, etc.
[29] J. De Coninck, U. D'Ortona, J. Koplik, and J. R. Banavar, *Phys. Rev. Lett.* **74**, 928 (1995).
[30] U. D'Ortona, J. De Coninck, J. Koplik, and J. R. Banavar, *Phys. Rev. E* **53**, 562 (1996).
[31] A. Lukkarinen, D. B. Abraham, M. Karttunen, and K. Kaski, *Phys. Rev. E* **51**, 2199 (1995).
[32] J. Van Alsten and S. Granick, *Phys. Rev. Lett.* **61**, 2570 (1988).
[33] H.-W. Hu, G. A. Carson, and S. Granick, *Phys. Rev. Lett.* **66**, 2758 (1991).
[34] M. L. Gee, P. M. McGuiggan, J. N. Israelachvili, and A. M. Homola, *J. Chem. Phys.* **93**, 1895 (1990).
[35] J. N. Israelachvili, *Intermolecular and Surface Forces* (Academic, London, 1985).
[36] P. A. Thompson, G. S. Grest, and M. O. Robbins, *Phys. Rev. Lett.* **68**, 3448 (1992).
[37] P. G. de Gennes and A. M. Cazabat, *C. R. Acad. Sci.* **310**, 1601 (1990).
[38] L. Wagner, *Phys. Rev. E* **52**, 2797 (1995).
[39] D. B. Abraham, P. Collet, J. De Coninck, and F. Dunlop, *Phys. Rev. Lett.* **65**, 195 (1990).
[40] D. B. Abraham, P. Collet, J. De Coninck, and F. Dunlop, *J. Stat. Phys.* **61**, 509 (1990).

- [41] J. De Coninck, F. Dunlop, and F. Menu, *Phys. Rev. E* **47**, 1820 (1993).
- [42] D. B. Abraham, in *Phase Transitions and Critical Phenomena*, edited by C. Domb and J. L. Lebowitz (Academic, New York, 1986), Vol 10.
- [43] S. F. Burlatsky, G. Oshanin, A. M. Cazabat, and M. Moreau, *Phys. Rev. Lett.* **76**, 86 (1996).
- [44] S. F. Burlatsky, W. Reinhardt, G. Oshanin, and M. Moreau, *Bull. Am. Phys. Soc.* **40**, 301 (1995).
- [45] S. F. Burlatsky, G. Oshanin, A. Mogutov, and M. Moreau, *Phys. Lett. A* **166**, 230 (1992).
- [46] S. F. Burlatsky, G. Oshanin, M. Moreau, and W. Reinhardt, *Phys. Rev. E* **54**, 3165 (1996).
- [47] R. Aveyard and D. A. Haydon, *An Introduction to the Principles of Surface Chemistry* (Cambridge University Press, Cambridge, 1973).
- [48] S. Alexander and P. Pincus, *Phys. Rev. B* **18**, 2011 (1978).
- [49] T. M. Liggett, *Interacting Particle Systems* (Springer-Verlag, New York, 1985).
- [50] J. S. Langer, in *Chance and Matter*, edited by J. Souletie, J. Vannimenes, and R. Stora (North-Holland, Amsterdam, 1987).
- [51] M. P. Valignat *et al.*, *Colloids Surf.* **83**, 193 (1994).